Flow Turbulence Combust (2014) 93:439–459
DOI 10.1007/s10494-014-9563-3

Topology and Brush Thickness of Turbulent Premixed V-shaped Flames

S. Kheirkhah · Ö. L. Gülder

Received: 19 December 2013 / Accepted: 29 July 2014 / Published online: 22 August 2014

Abstract Topology and brush thickness of turbulent premixed V-shaped flames were investigated using Mie scattering and Particle Image Velocimetry techniques. Mean bulk flow velocities of 4.0, 6.2, and 8.3 m/s along with two fuel-air equivalence ratios of 0.6 and 0.7 were tested in the experiments. Using a novel experimental turbulence generating apparatus, three turbulence intensities of approximately 2 %, 6 %, and 17 % were tested in the experiments. The results show that topology of the flame front is significantly altered by changing the turbulence intensity. Specifically, at relatively small turbulence intensities, the flame fronts feature wrinkles which are symmetric with respect to the vertical axis. At moderate values of turbulence intensities, the flame fronts form cusps. The formation of cusps is more pronounced at large mean bulk flow velocities. The results associated with relatively large turbulence intensity show that flame surfaces feature: mushroom-shaped structures, freely propagating sub-flames, pocket formation, localized extinction, and horn-shaped structures. Analysis of the results show that the flame brush thickness follows a linear correlation with the root-mean-square of the flame front position. The correlation is in agreement with the results of past experimental investigations associated with moderately turbulent premixed V-shaped flames, and holds for the range of turbulence conditions tested. This suggests that the underlying mechanism associated with the dynamics of moderately turbulent premixed V-shaped flames proposed in past studies can potentially be valid for the the wide range of turbulence conditions examined in the present investigation.

Keywords Turbulent premixed combustion · Flame front topology · Flame brush thickness

1 Introduction

Several engineering systems, e.g., stationary gas turbines, lean premixed and prevaporized gas turbine engines, and spark ignition engines perform in the mode of turbulent

S. Kheirkhah (✉) · Ö. L. Gülder
University of Toronto Institute for Aerospace Studies, Toronto, Ontario M3H 5T6, Canada
e-mail: kheirkhah@utias.utoronto.ca

premixed combustion [1–4]. The combustion processes in these engineering applications are accompanied by significantly large values of turbulence intensities ($u'/U \sim 50$ %), where u' and U are the root-mean-square (RMS) and mean of the velocity measured in the reactants flow [5]. In several investigations associated with turbulent premixed combustion, the V-shaped flame configuration has been utilized to study the fundamental physics associated with combustion processes in real engineering applications; see, for example, the review papers by Clavin [3] and Driscoll [4]. Survey of literature pertaining to V-shaped flames shows that perforated plates or mesh screens have been mainly utilized for turbulence generation purposes. These apparatuses can generate turbulent flow fields with corresponding turbulence intensities of about 10 %. The values of turbulence intensities associated with perforated plates and mesh screens are significantly smaller than those pertaining to real engineering applications. Since the flame characteristics can become strongly altered at large values of u'/U, the present study is motivated by the need to explore the turbulent premixed V-shaped flame characteristics at relatively large values of turbulence intensities. In this investigation, two characteristics are studied: flame front topology and flame brush thickness. The rest of this section presents a review of literature associated with these characteristics.

Studying the flame front topology is associated with realization of flame front structures apparent in turbulent premixed flames. The flame front structures are of significant importance since they are related to several flame front characteristics, e.g., flame front curvature, surface density, and brush thickness. Thus, several investigations have been performed to study the topology of V-shaped flames in the past decades; see, for example, [6–10]. Experimental results presented in Goix et al. [6] show that, for relatively small values of turbulence intensities, therein referred to as laminar condition, the flame fronts represent two straight lines. At relatively moderate values of turbulence intensity, i.e., $u'/U \sim 10$ %, results presented in [6–10] show that the topology of turbulent premixed V-shaped flames depends on the vertical distance from the flame-holder. Relatively close to the flame-holder, similar to the results associated with small values of u'/U, the flame fronts feature two straight lines. However, at large vertical distances from the flame-holder, the flame fronts become wrinkled [6–10]. Although topology of turbulent premixed V-shaped flames is investigated for relatively small and moderate values of turbulence intensities [6–10], it is not studied for relatively large values of turbulence intensities.

The flame brush thickness (δ_T) is an approximate distance over which the flame front exists [4]. In turbulent premixed V-shaped flames, δ_T can be estimated using the following equation [9]:

$$\delta_T = \frac{1}{\max(-\mathrm{d}\overline{c}/\mathrm{d}x)}, \tag{1}$$

where $\overline{c}$ is the mean-progress-variable, and x is the axis normal to the vertical axis pointing towards the reactants region. Two mathematical formulations have been developed for the flame brush thickness in the literature. The first formulation is associated with the Langevin model [11, 12]. Taylor also proposed a similar formulation in his turbulent diffusion theory [13]. Using the results provided in [11–13], it is shown [4, 14, 15] that the flame brush thickness normalized by the integral length scale (δ_T/Λ) can be obtained from the following formulation:

$$\frac{\delta_T}{\Lambda} = \sqrt{2\pi}\{2\frac{t}{\tau}\{1 - \frac{\tau}{t}[1 - \exp(-\frac{t}{\tau})]\}\}^{\frac{1}{2}}. \tag{2}$$

Note that the factor $\sqrt{2\pi}$ is missing in [4, 14]. In Eq. 2, t is referred to as the eddy convection time and equals to the ratio of the vertical distance from the flame-holder (y) to the mean bulk flow velocity (U) [4]. τ is referred to as the eddy turnover time and equals to Λ/u' [4]. The second formulation developed for the flame brush thickness is associated with the level set formalism [1]. Peters [1] shows that the flame brush thickness can be obtained from the following equation:

$$\frac{\delta_T}{\Lambda} = 1.78[1 - \exp(-2\frac{t}{\tau})]^{\frac{1}{2}}. \tag{3}$$

It can be shown that both Eqs. 2 and 3 predict a linear correlation between the normalized flame brush thickness and the normalized convection time (t/τ) for relatively small values of this parameter. For relatively large values of t/τ, Eq. 2 suggests that $\delta_T/\Lambda = 2\sqrt{\pi t/\tau}$, while Eq. 3 predicts $\delta_T/\Lambda = 1.78$.

Guo et al. [8], Kheirkhah and Gülder [9], Namazian et al. [16], and Rajan et al. [17] experimentally investigated the flame brush thickness of turbulent premixed V-shaped flames. Their results show that δ_T is dependent on the vertical distance from the flame-holder, turbulence intensity, and the fuel-air equivalence ratio (ϕ). Specifically, their results show that increasing y and u'/U increases the flame brush thickness. This is in agreement with the formulations presented in Eqs. 2 and 3. The results of past experimental investigations [8, 9, 16] show that increasing the fuel-air equivalence ratio increases the flame brush thickness. Kheirkhah and Gülder [9] showed that the flame brush thickness is proportional to the root-mean-square (RMS) of the flame front position (x'); and x' increases with increasing the fuel-air equivalence ratio. Also, in a recent publication [10], the authors discuss that the reason for the increase of x' with ϕ is the enhancement of the reactants transverse velocity fluctuations at the vicinity of the flame front. Thus, the reason for the increase of δ_T with ϕ is known for moderately turbulent premixed V-shaped flames. Nevertheless, increase of δ_T with ϕ is in contrast with predictions of both models presented in Eqs. 2 and 3. As speculated by Lipatnikov and Chomiak [14], this discrepancy between the experimental results and those of theoretical formulations may be attributed to the formulations not being capable of incorporating the effect of heat release on the flame front dynamics.

To the best knowledge of the authors, topology of turbulent premixed V-shaped flames as well as the flame brush thickness have not been investigated for relatively large values of turbulence intensities, i.e., $u'/U \sim 20$ %. Specifically, the validity of the linear correlation between δ_T and x', proposed in Kheirkhah and Gülder [9] for moderate values of u'/U, has not been investigated for relatively large values of u'/U. The present study aims at developing a novel experimental apparatus which allows for producing relatively large values of u'/U. Then, topology of turbulent premixed V-shaped flames as well as the flame brush thickness are investigated for the large values of turbulence intensity. For comparison purposes, the flame front characteristics are also studied at small and moderate values of u'/U.

2 Experimental Methodology

This section consists of the experimental setup utilized for producing the V-shaped flames, the measurement techniques, and the experimental conditions tested.

2.1 Experimental setup

Burner setup and coordinate system The V-shaped flames were produced using the burner shown in Fig. 1a. The burner is composed of an expansion section, a settling chamber, a contraction section, and a nozzle. The expansion section has an expansion area ratio of about four. As can be seen from Fig. 1a, a baffle disk is placed close to the entrance of the expansion section in order to disperse the entering premixed and seeding flows. Following the expansion section, a settling chamber is placed. The chamber contains five mesh screens for flow conditioning purposes. After the settling chamber, a contraction section with a contraction area ratio of about seven is placed. A nozzle section is installed after the contraction section. The nozzle has an inner diameter (D) of 48.4 mm. A flame-holder is placed close to the exit of the nozzle, see Fig. 1b. The flame-holder is cylindrical in shape, and has a diameter (d) of 2 mm. A flame-holder support was used to fix the flame-holder, see Fig. 1b. Parallel and circular guiding holes were generated on the flame-holder support. The guiding holes serve as a sliding mechanism which allows for adjusting the distance between the flame-holder centerline and the exit plane of the burner, see Fig. 1b. This distance was fixed at 4 mm for all the experimental conditions tested.

The coordinate system utilized in the present investigation is Cartesian, as shown in Fig. 1b. The origin of the coordinate system is located equidistant from both ends of the flame-holder, and 5 mm above the burner exit plane. The y-axis of the coordinate system is normal to the exit plane of the burner. The x-axis is normal to both y-axis and the flame-holder centreline. The z-axis is normal to both x and y axes and lies along the span of the flame-holder.

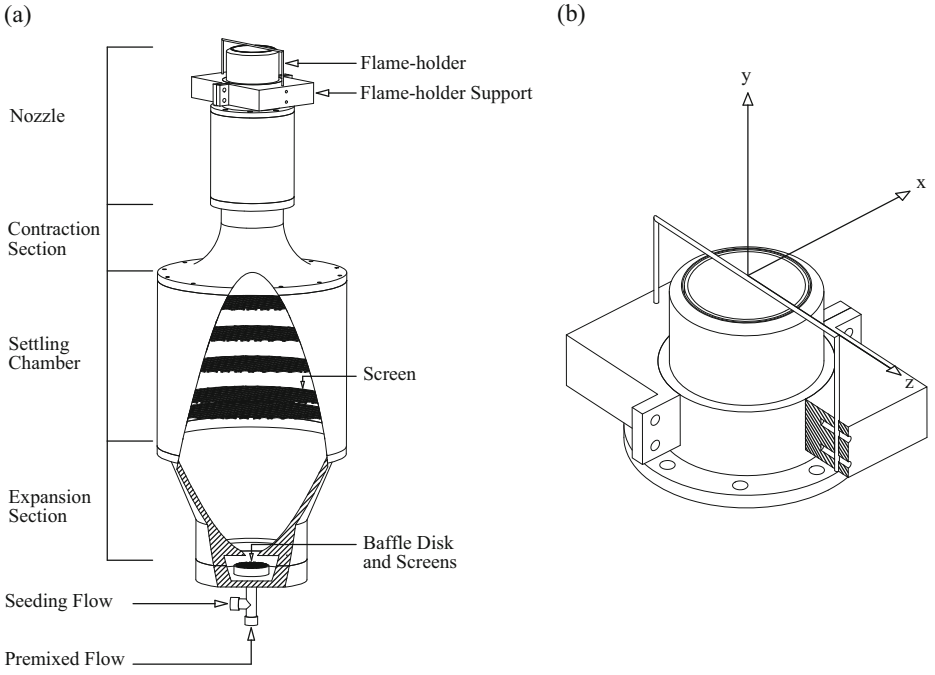

Fig. 1 **(a)** Burner setup and **(b)** flame-holder, flame-holder support, and coordinate system details

Turbulence generating arrangements Three turbulence generating arrangements were utilized in the present study. For the first arrangement, turbulence was produced by the mesh screens in the settling chamber, see Fig. 1a. The values of the turbulence intensities pertaining to this arrangement were relatively small ($u'/U \approx 0.02$). Relatively moderate and large values of turbulence intensities were produced using the second and the third arrangements, with details provided below.

The technical drawing associated with the second turbulence generation arrangement is presented in Fig. 2a. The generator shown in Fig. 2a is a stainless steel perforated plate, with outer diameter (D) of 48.4 mm and a thickness of 1 mm. Sixty seven circular holes were generated on the plate. The holes are arranged in hexagonal pattern. Each hole has a diameter (D_h) of 3.9 mm. The distance between two neighbouring holes (s) is 5.7 mm. This arrangement of holes results in a plate blockage ratio of approximately 58 %. The turbulence intensity pertaining to the second arrangement is $u'/U \approx 0.06$.

Figure 2b represents the technical drawing of the third turbulence generation arrangement. The generator shown in Fig. 2b is composed of two perforated plates, with the plate technical drawing presented in Fig. 2a. In Fig. 2b, r and θ are the distance between two

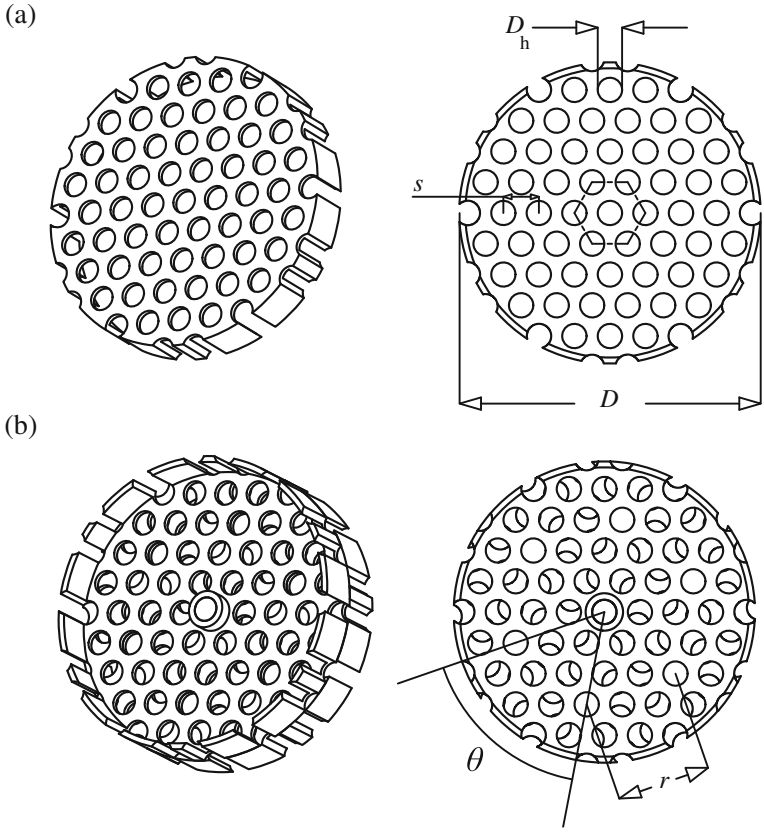

Fig. 2 **(a)** and **(b)** Turbulence generating mechanisms utilized for the second and the third arrangements, respectively

neighbouring circular holes as well as the relative angular position of the plates, respectively. The results show that both r and θ significantly affect the turbulent flow characteristics. Using a trial and error technique, these parameters were tuned such that the turbulence intensity produced by the arrangement is maximized. The pertaining values of r and θ are approximately 15 mm and 60°, respectively. This arrangement results in a turbulence intensity of $u'/U \approx 0.17$.

Depending on the second or third turbulence generating arrangement tested, either the generator shown in Fig. 2a or that shown in Fig. 2b was placed in the nozzle section of the burner. For distances between the turbulence generating mechanism and the exit plane of the nozzle smaller than about 50 mm, the flames occasionally flash back and stabilize on the turbulence generating mechanism rather than the flame-holder. In order to avoid this problem, for the second and the third arrangements, the turbulence generators were placed one and a half nozzle diameters, i.e., about 73 mm, upstream of the nozzle exit plane.

2.2 Measurement techniques

The Mie scattering and the Particle Image Velocimetry (PIV) techniques were utilized in the experiments. The former was used to study the flame front topology and flame brush thickness. The latter was utilized for estimating the velocity field characteristics under non-reacting flow conditions. The following two subsections provide details associated with the measurement techniques.

Mie scattering Mie scattering is elastic scattering of light, with wavelength λ, from particles with average size d_p, when $d_p \gtrsim \lambda$ [18]. Olive oil droplets were utilized for seeding purposes in the Mie scattering experiments. A Laskin-nozzle type nebulizer utilized in past investigations [9, 19, 20] was used for producing the olive oil droplets.

In the application of the Mie scattering technique for studying premixed combustion, it is assumed that the combustion occurs inside a relatively thin layer. This assumption is referred to as the flamelet assumption [21]. Implication of the flamelet assumption is that if the reactants are seeded with particles which evaporate at the flame front, the light intensities scattered from the particles significantly change across the flame front. This abrupt change in the light intensities was used for obtaining the flame front in the present study.

The hardware associated with the Mie scattering technique consists of a CCD camera and a pulsed Nd:YAG laser. The CCD array has a resolution of 2048 pixels $\times$ 2048 pixels. The camera head is equipped with a Macro lens which has a focal length (f) of 105 mm. For all experiments, the lens aperture size was fixed at $f/8$. Also, the lens was equipped with a 532 nm band-pass filter in order to avoid influence of flame chemiluminescence in the acquired images.

The flow field was illuminated by a laser sheet formed from a 6.5 mm diameter beam, which has a wavelength of 532 nm, a beam energy of about 120 mJ per pulse, and a pulse duration of about 4 ns. At the plane of $z/d = 0$, where all the experiments were performed, the laser sheet thickness was measured to be $150 \pm 50 \mu m$. The laser operated at a frequency of 5 Hz and the Mie scattering images were simultaneously acquired by the CCD camera. For statistical analysis purposes, 1000 images were acquired for each experimental condition tested. The recorded images were binarized and filtered using the algorithm detailed in Kheirkhah and Gülder [9].

Particle image velocimetry The Particle Image Velocimetry (PIV) was performed in order to estimate the non-reacting turbulent flow characteristics. The hardware associated with

the PIV is identical to that used for the Mie scattering experiments. Also, similar to the Mie scattering experiments, olive oil droplets were utilized for seeding purposes in the PIV experiments. For each experimental condition tested, 1000 PIV image pairs were acquired. The interrogation box size was set to be 16 pixels, with zero overlap between the boxes. The separation time between the laser pulses, was selected such that the average distance traced by the seeding particles in each interrogation box was approximately 25 % of the size of the interrogation box. This measure was taken in order to avoid particles loss between consecutive images.

2.3 Experimental conditions

The tested experimental conditions are tabulated in Table 1. Methane grade 2, i.e., methane with 99 % chemical purity, was used as the fuel in the experiments. All velocity statistics presented in Table 1 were estimated using the Particle Image Velocimetry (PIV) technique for non-reacting flow condition and without the flame-holder in place. The velocity data were estimated along the line associated with the intersection of the planes: $y/d = -1$ and $z/d = 0$. Then, mean and RMS of the streamwise velocity data were averaged along the corresponding line (from $x/d = -12$ to 12). In Table 1, U and u'/U pertain to the averaged values along the x-axis. In the table, Flames A-F, G-L, and M-R correspond to the first, the second, and the third turbulence generating arrangements, respectively. For each turbulence generating arrangement, three mean bulk flow velocities of $U = 4.0$, 6.3, and 8.3 m/s were tested. For each mean bulk flow

Table 1 Tested experimental conditions

	U(m/s)	ϕ	S_{L0}(m/s)	δ_L(mm)	u'/U	Λ(mm)	Re_Λ	Da	Ka
Flame A	4.0	0.6	0.13	0.17	0.02	2.6	13.2	24.8	0.02
Flame B	4.0	0.7	0.20	0.11	0.02	2.6	13.2	58.8	0.01
Flame C	6.2	0.6	0.13	0.17	0.02	2.5	17.5	17.4	0.03
Flame D	6.2	0.7	0.20	0.11	0.02	2.5	17.5	41.1	0.01
Flame E	8.3	0.6	0.13	0.17	0.02	2.4	30.6	9.2	0.07
Flame F	8.3	0.7	0.20	0.11	0.02	2.4	30.6	21.7	0.03
Flame G	4.0	0.6	0.13	0.17	0.06	4.2	58.9	14.6	0.06
Flame H	4.0	0.7	0.20	0.11	0.06	4.2	58.9	34.5	0.02
Flame I	6.2	0.6	0.13	0.17	0.06	3.8	84.7	8.3	0.12
Flame J	6.2	0.7	0.20	0.11	0.06	3.8	84.7	19.6	0.05
Flame K	8.3	0.6	0.13	0.17	0.06	3.8	116.2	6.1	0.20
Flame L	8.3	0.7	0.20	0.11	0.06	3.8	116.2	14.3	0.08
Flame M	4.0	0.6	0.13	0.17	0.18	6.3	284.9	6.8	0.28
Flame N	4.0	0.7	0.20	0.11	0.18	6.3	284.9	16.1	0.12
Flame O	6.2	0.6	0.13	0.17	0.17	5.5	429.4	4.5	0.51
Flame P	6.2	0.7	0.20	0.11	0.17	5.5	429.4	10.7	0.22
Flame Q	8.3	0.6	0.13	0.17	0.17	5.5	501.0	2.9	0.85
Flame R	8.3	0.7	0.20	0.11	0.17	5.5	501.0	7.0	0.36

velocity, two fuel-air equivalence ratios of $\phi = 0.6$ and 0.7 were examined. It was desirable to perform experiments at larger values of fuel-air equivalence ratio, e.g., $\phi = 0.8$ and $\phi = 0.9$. However, due to occasional flash back of the flames associated with the third turbulence generation arrangement for $\phi \gtrsim 0.7$, experiments were not performed for fuel-air equivalence ratios larger than 0.7. In Table 1, the integral length scale (Λ) was estimated from the autocorrelation of the streamwise velocity data calculated along the y-axis [12]. The values of the unstretched laminar flame speed was extracted from [22]. The laminar flame thickness was estimated from $\delta_L = \mathcal{D}/S_{L0}$, where $\mathcal{D} = \nu/(PrLe)$. The Lewis number (Le), the Prandtl number (Pr), and the kinematic viscosity (ν) are estimated for the reactants at standard temperature and pressure conditions. Le, Pr, and ν are unity, 0.71, and $1.57 \times 10^{-5}\text{m}^2/\text{s}$, respectively. In Table 1, Reynolds, Damköhler, and Karlovitz numbers are calculated from $Re_\Lambda = u'\Lambda/\nu$, $Da = S_{L0}\Lambda/(u'\delta_L)$, and $Ka = 0.157(u'/S_{L0})^2 Re_\Lambda^{-0.5}$ [23], respectively.

All the experimental conditions tested are overlaid on the Borghi diagram [1], presented in Fig. 3. As shown in the figure, the experimental conditions associated with the first, the second, and the third turbulence generation arrangements mainly correspond to the wrinkled flames, the corrugated flames, and the thin reaction zones, respectively.

3 Results

The results are associated with the flame front topology and the flame brush thickness. The Mie scattering technique was utilized to obtain the data associated with these characteristics. The Mie scattering is a two-dimensional imaging technique. It is believed that the three-dimensionality of the flame surfaces enhances with increasing the turbulence intensity.

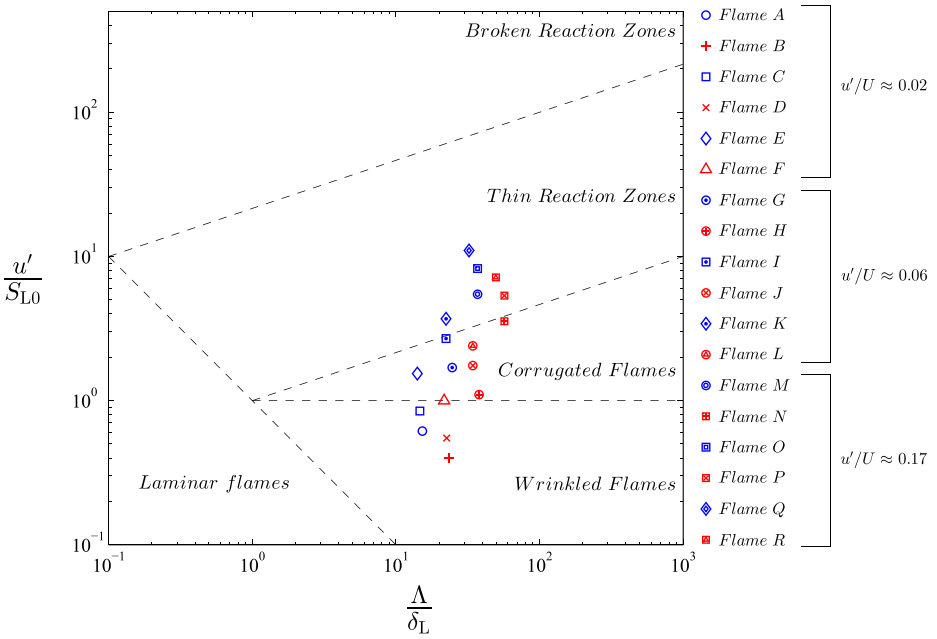

Fig. 3 The experimental conditions overlaid on the Borghi diagram [1]

However, the three-dimensionality of the flame surfaces does not influence the discussions presented in here. This is because the results pertaining to the flame front topology provide qualitative presentation of the flame surfaces as apposed to quantitative presentations. For the flame brush thickness, by definition, δ_T depends on the characteristics of the mean-progress-variable measured at a single plane ($z/d = 0$), see Eq. 1. Although, values of δ_T can potentially vary in planes of $z/d \neq 0$, the values measured at $z/d = 0$ are independent of three-dimensionalty of the flame fronts. In the following sections, first, the results associated with the flame front topology are presented. Then, the flame brush thickness is studied.

3.1 Flame front topology

Analysis of the Mie scattering images shows that, for all experimental conditions tested, the topology of the flame fronts strongly depends on the turbulence intensities examined. Three representative Mie scattering images associated with relatively small, moderate, and large values of turbulence intensities are shown in Fig. 4a, b and c, respectively. The flame fronts are shown by the highlighted curves in the figures. The results in Fig. 4a show that, at relatively small value of the turbulence intensity, the flame fronts represent two straight lines. However, the results in Fig. 4b and c show that, at relatively moderate and large values of turbulence intensity, the flame fronts are wrinkled. The results in Fig. 4a–c show that increasing the turbulence intensity increases the wrinkling of the flame surfaces. In addition to enhancement of the flame front wrinkling, increasing u'/U from moderate to large values results in spread of the flame surfaces in a relatively larger area. Since the topology of the turbulent premixed V-shaped flames shows a strong dependence on u'/U, the results are discussed in three subsections: small, moderate, and large values of turbulence intensities.

Small turbulence intensity For the experimental conditions associated with relatively small turbulence intensities (Flames A-F), the Mie scattering images show that the flame fronts mainly feature two straight lines similar to the results presented in Fig. 4a. The results in the figure showed that the flame fronts are symmetric with respect to the y-axis.

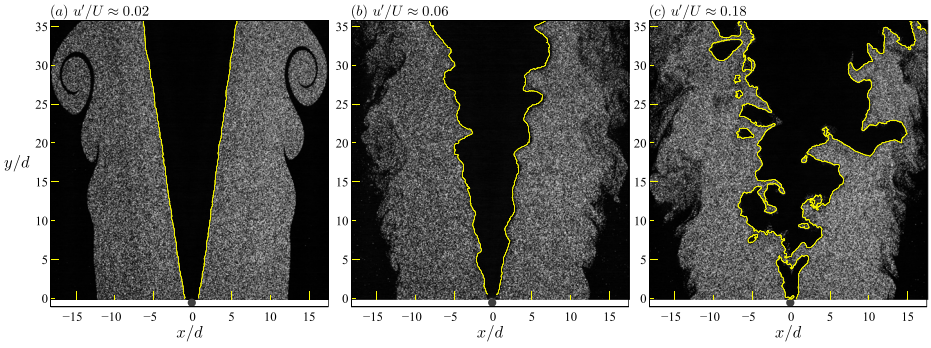

Fig. 4 Representative images of the flame front topology. **(a)**, **(b)**, and **(c)** correspond to Flames A, G, and M, respectively. The turbulence intensities associated with **(a)**, **(b)**, and **(c)** are $u'/U = 0.02$, 0.06, and 0.18, respectively. For all flame conditions presented, the the mean bulk flow velocity and the fuel-air equivalence ratio are fixed at $U = 4.0$ m/s and $\phi = 0.6$, respectively

This is similar to the results associated with relatively small values of turbulence intensity presented in Goix et al. [6].

In comparison to the results presented in Fig. 4a, which showed two straight lines, the analysis of the Mie scattering images show that, with increasing the mean bulk flow velocity, the flame fronts become perturbed. The perturbations are more pronounced at large vertical distances from the flame-holder. Representative flame fronts featuring two perturbed lines, corresponding to Flame F condition, are presented in Fig. 5a. As shown in the figure, relatively close to the flame-holder ($y/d \lesssim 5$), the flame fronts feature two straight lines. However, for $y/d \gtrsim 5$, the amplitude of the perturbations grows towards the downstream direction. Two insets of Fig. 5a, associated with the left and right wings of the flame fronts, are presented in Fig. 5b and c, respectively. The results in Fig. 5b and c show that the flame fronts are symmetric with respect to the y-axis. Shanbhogue et al. [24] investigated topology of V-shaped flames in both presence and absence of acoustic excitation. For relatively small turbulence intensities and without the excitation, in agreement with the results presented in Fig. 5a, their results [24] show that the flame fronts feature corrugated surfaces that are symmetric with respect to the vertical axis.

Moderate turbulence intensity Comparison of the results presented in Fig. 4a and b showed that increasing the turbulence intensity from about 2 % to 6 % strongly affects topology of the turbulent premixed V-shaped flames. Specifically, the symmetry of the flame fronts observed for relatively small values of turbulence intensity disappears at moderate values of u'/U. Since the characteristics of the reactants flow are expected to influence topology of the flame fronts, the asymmetry of the flame fronts pertaining to relatively moderate

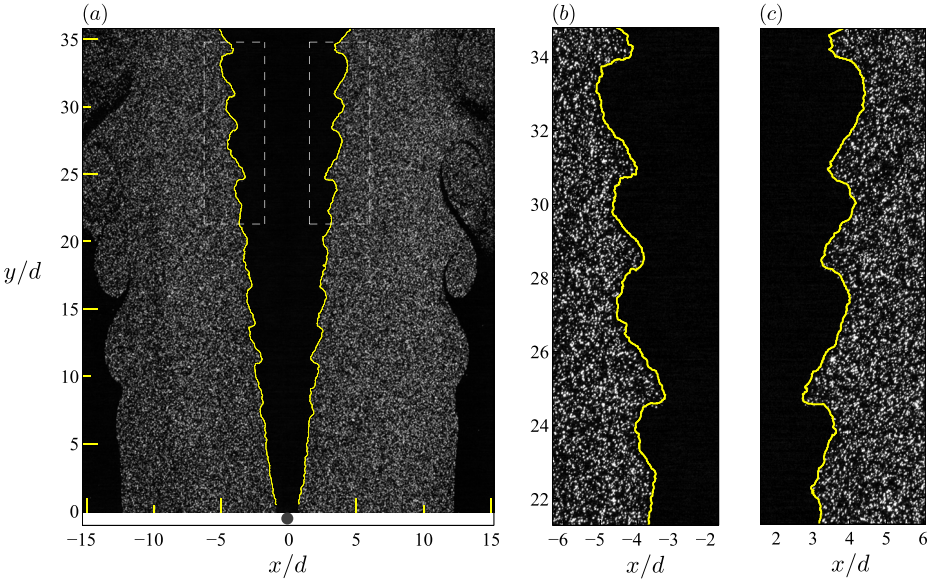

Fig. 5 **(a)** Representative Mie scattering image associated with Flame F condition. The corresponding mean bulk flow velocity, turbulence intensity, and fuel-air equivalence ratio are $U = 8.3$ m/s, $u'/U = 0.02$, and $\phi = 0.7$, respectively. **(b)** and **(c)** are insets of **(a)** and correspond to the left and right wings of the flame front, respectively

value of u'/U is linked to relatively strong velocity fluctuations associated with Flames G-L conditions.

Although topology of the flame surfaces changes by increasing the turbulence intensity from about 2 % to 6 %, the flame fronts associated with the relatively small and moderate values of u'/U feature common characteristics. Specifically, comparison of the results presented in Fig. 4b with those in Fig. 5, show that size of flame front wrinkles increases with increasing the vertical distance from the flame-holder. This indicates that, for the experimental conditions corresponding to Flames A-F and G-L, the flame brush thickness is expected to increase by increasing the vertical distance from the flame-holder. Indeed, results of past studies associated with relatively small and moderate values of u'/U show that increasing y increases δ_T, see, for example, [9].

In addition to the similarity associated with the growth of the size of the wrinkles with vertical distance from the flame-holder, comparison of the results presented in Figs. 4b and 5a shows formations of cusps for experimental conditions associated with both relatively small and moderate values of turbulence intensity. Cusps are flame front structures with negative and large values of curvature [25], where negative value of curvature refers to the flame front being concave towards the reactants region [25]. Analysis of the Mie scattering images associated with Flames A-F and G-L show that the formation of cusps is more pronounced both at relatively large values of mean (U) and RMS (u') velocity fluctuations. A representative Mie scattering image associated with the experimental condition of Flame L is shown in Fig. 6a. The regions associated with cusp formations are highlighted by the

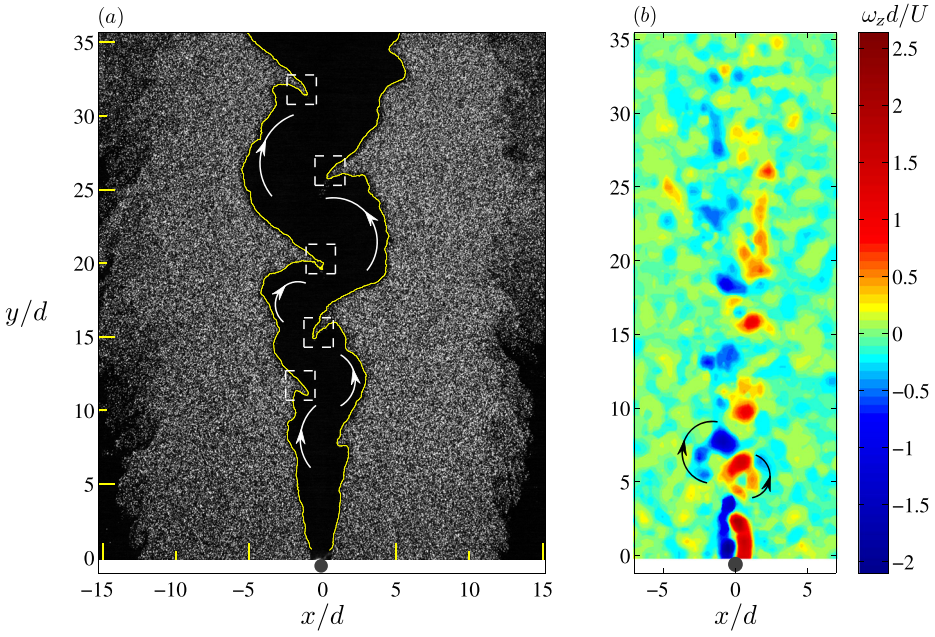

Fig. 6 **(a)** Representative flame front associated with Flame L condition, with $U = 8.3$ m/s, $u'/U = 0.06$, and $\phi = 0.7$. The white dashed boxes highlight the regions of cusp formation. The white curved arrows correspond to possible directions of vortices rotations. **(b)** Representative normalized vorticity contour of non-reacting flow, with experimental conditions identical to those of **(a)**

dashed boxes in the figure. Figure 6b represents normalized vorticity ($\omega_z d/U$) contours in the wake of the flame-holder and for non-reacting flow condition. The turbulence characteristics at the exit of the burner ($y/d \approx -1$) are identical for the results presented in both Figure 6a and b. The results presented in Fig. 6b indicate that the flow structure in the wake of the flame-holder is dominated by alternate shedding of vortices, with representative direction of rotations shown by the black curved arrows in Fig. 6b. Although, for reacting flow condition, due to heat release effects, the flow structures shown in Fig. 6b may alter, previous studies, e.g., [26], show that the vortex shedding exists in the wake of the flame-holder. This observation is also confirmed by studies associated with turbulent premixed flames stabilized in the wake of non-circular flame-holders; see, for example, [24]. The studies of [24, 26] indicate that the flow structures strongly influence the flame fronts. Specifically, the results presented in [24] show that the vortices are mainly surrounded by the flame surfaces. This interaction of vortices and the flame front is speculated to affect the flame front topology presented in Fig. 6a. The flame fronts shown in Fig. 6a seem to surround boundaries of a von Kármán vortex street. Possible direction of vortices rotations are shown by the white curved arrows in the figure. The results in Fig. 6a suggest that the cusps are formed due to the interaction between the flame fronts and the vortices formed in the wake of the flame-holder.

Large turbulence intensity Results presented in previous subsections show that certain flame front structures can be identified using the Mie scattering technique. This is due to the state of the flow being associated with relatively small and moderate values of turbulence intensities. In comparison to flame topology associated with relatively small and moderate values of u'/U, for large values of turbulence intensity, the flame fronts become significantly disturbed, see Fig. 4c. Although the results in Fig. 4c show that the flame fronts seem to be significantly disordered, analysis of the Mie scattering images suggests that the flame fronts feature certain characteristics. Qualitative study of these characteristics is of importance since it can provide insight into quantitative arguments pertaining to turbulent premixed V-shaped flames. Specifically, the arguments provided in this section can be potentially utilized for understanding several flame front characteristics associated with highly turbulent premixed V-shaped flames, e.g., flame front curvature and flame brush thickness.

A representative Mie scattering image corresponding to relatively large value of turbulence intensity is presented in Fig. 7a. The results in the figure show formation of certain flame front structures, with details provided below.

I. Mushroom-shaped flame front structures Flame front structures similar to those presented in Fig. 7b are commonly observed in the Mie scattering images associated with relatively large values of turbulence intensities (Flames M-R), and are referred to as mushroom-shaped flame front structures. Figure 7b contains two mushroom-shaped flame front structures: one oriented towards the reactants region and the other oriented towards the products region, see Fig. 7b.

Formations of flame front structures, similar to those presented in Fig. 7b, are previously observed and reported for Bunsen flames (see, for example, Buchmann et al. [27]), opposed jet flames (see, for example, Coriton et al. [28]), and swirl stabilized flames (see, for example, Cheng et al. [29]). The experimental conditions investigated in [27–29], similar to those of the Flames M-R of the present study, mainly correspond to the thin reaction zones regime. Thus, it is speculated that the formation of the mushroom-shaped flame structure

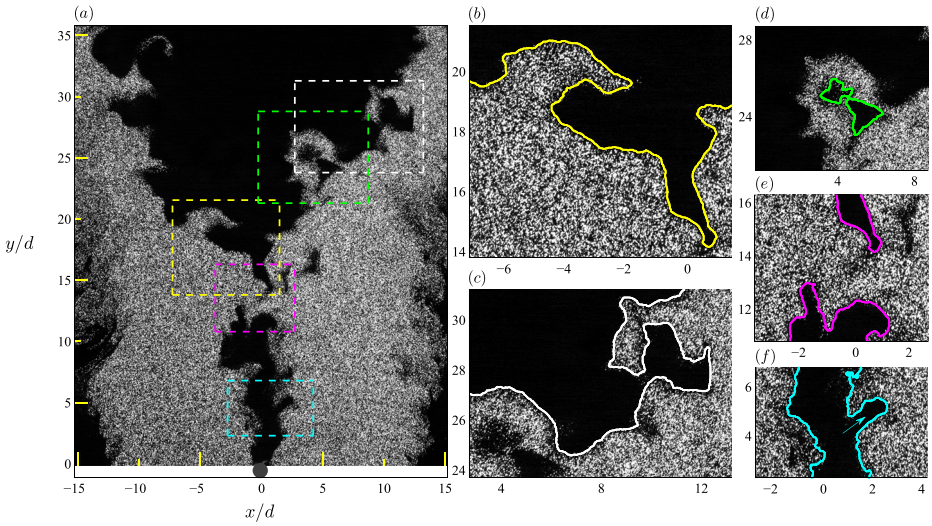

Fig. 7 **(a)** Representative Mie scattering image pertaining to Flame M condition, with $U = 4.0$ m/s, $u'/U = 0.18$, and $\phi = 0.6$. **(b)**, **(c)**, **(d)**, **(e)**, and **(f)** pertain to mushroom-shaped flame structure, freely propagating sub-flames, pocket formation, localized extinction, and horn-shaped flame front structure, respectively

is independent of the flame geometry and is a characteristic of turbulent premixed flames associated with the thin reaction zones regime.

II. Freely propagating Sub-flames The results show that, at relatively large values of turbulence intensities, the V-shaped flames consist of flame front structures similar to that shown in Fig. 7c. These structures do not feature a specific orientation with respect to the reactants flow, and are referred to as freely propagating sub-flames. These sub-flames are usually composed of more than one mushroom-shaped flame structure, see Fig. 7c. Topology of the freely propagating sub-flames is similar to that of swirl stabilized flames; see, for example, the results presented in Cheng et al. [29].

III. Pocket formation Analysis of the Mie scattering images shows formations of both pockets of products in the reactants region and pockets of reactants in the products region. This phenomenon mainly takes place at relatively large vertical distances from the flame-holder. Figure 7d represents an enlarged inset of Fig. 7a associated with formation of pockets of products in the reactants region. The pocket formation is a characteristic of turbulent premixed flames and is previously observed for Bunsen flames [27], opposed jet flames [28], and swirl stabilized flames [29]. Similar to the formation of mushroom-shaped structures, pocket formation is speculated to be independent of the flame geometry, and is a characteristic of turbulent premixed flames pertaining to the regime of thin reaction zones.

Analysis of the Mie scattering images shows that two relatively rare phenomena associated with pocket formation may happen for the flames pertaining to large values of turbulence intensities. First, pocket formation may rarely happen at relatively small vertical distances from the flame-holder. A representative image associated with this phenomenon is presented in Fig. 8a. A similar observation, pertaining to that presented in Fig. 8a, is previously reported for V-shaped flames; see, for example, [30]. The second rare

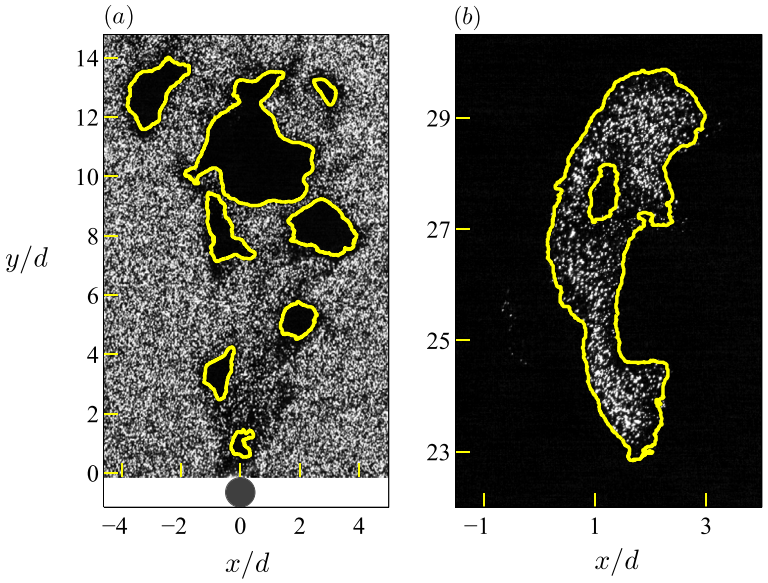

Fig. 8 **(a)** Pocket formation close to the flame-holder. **(b)** Formation of a pocket of products inside a pocket of reactants. The results in both **(a)** and **(b)** correspond to Flame O condition, with $U = 6.2$ m/s, $u'/U = 0.17$, and $\phi = 0.6$

phenomenon is associated with formation of a pocket of products inside a pocket of reactants, with a representative image presented in Fig. 8b. These phenomena rarely happen and are attributed to relatively large values of turbulence intensities tested.

VI. Localized extinction The Mie scattering images show that, at relatively large values of u'/U, the V-shaped flames may become locally extinct. A representative image associated with the localized extinction is presented in Fig. 7e. This phenomenon leads to formations of two flames. One flame is located close and attached to the flame-holder, and the other flame is located at relatively large vertical distances and detached from the flame-holder, see Fig. 7e. The localized extinction phenomenon is previously observed in V-shaped flames, see e.g., [30–32]; and the terminology is adopted from [30]. Arguments provided in Shanbhogue et al. [30] indicate that the localized flame extinction is associated with relatively large values of flame stretch at the flame fronts. As discussed in [30], the local extinction results in dilution of the reactants with hot products, which significantly increases the local burning rate. The increased value of local burning rate results in re-ignition of the reactants and stabilization of the flames.

V. Formation of Horn-shaped flame front structures As shown in Fig. 7f, at relatively small vertical distances from the flame-holder, flame fronts may become significantly corrugated forming small scale flame front structures. These are approximately one cylinder diameter in size, formed on either the left or the right wing of the flame front, oriented towards the downstream direction, and are referred to as the horn-shaped flame front structures. Since these structures are relatively small and convex towards the reactants region, they are accompanied by large and positive values of curvature. Formation of relatively large and positive values of curvature has been previously observed and investigated in the past

studies, see, for example, [33]. As discussed in [33], formations of flame structures with large and positive values of curvature are due to interaction of the flame front with two counter-rotating vortices which pull the flame front towards the reactants region.

3.2 Flame brush thickness

For all experimental conditions tested, the flame brush thickness was estimated using Eq. 1. For both right and left wings of the flame front, variation of the flame brush thickness along the vertical axis is presented in Fig. 9a–i. The results in the first, the second, and the third columns correspond to mean bulk flow velocities of 4.0, 6.2, and 8.3 m/s, respectively. Also, the first, the second, and the third rows correspond to turbulence intensities of about 0.02, 0.06, and 0.17, respectively. In each figure, the blue color pertains to $\phi = 0.6$; and the red color corresponds to $\phi = 0.7$.

As shown in Fig. 9, both the turbulence intensity and the fuel-air equivalence ratio can influence the flame brush thickness. The results in Fig. 9 show that increasing the turbulence intensity increases the flame brush thickness. For example, at $y = 20$ mm, comparison of the results associated with Flames A, G, and M show that increasing the turbulence intensity from 2 % to 6 %, and 18 % increases the flame brush thickness from about 0.5 to 1.5, and 5 mm, respectively. For relatively small and moderate values of turbulence intensity, comparison of the flame front topology presented in Fig. 4a and b shows that the increase of the flame brush thickness with turbulence intensity is attributed to the pronounced wrinkling of the flame surfaces. Increasing the turbulence intensity to relatively large values

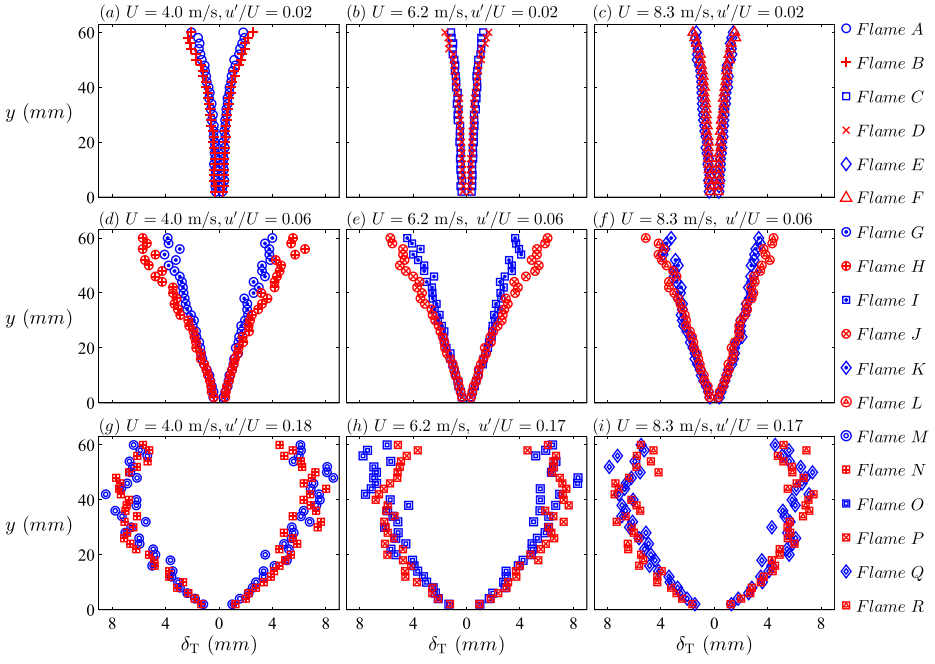

Fig. 9 Flame brush thickness. The first, the second, and the third rows correspond to $u'/U \approx 0.02$, 0.06, and 0.17; and, the first, the second, and the third columns pertain to mean bulk flow velocities of $U = 4.0$, 6.2, and 8.3 m/s, respectively. The blue and the red data symbols represent $\phi = 0.6$ and 0.7, respectively

causes further enhancement of the flame front wrinkling as well as formation of flame front structures detailed in the previous section. These two mechanisms cause significant increase of the flame brush thickness with increase of u'/U from relatively moderate to large values.

As can be seen from Fig. 9, influence of the fuel-air equivalence ratio on the flame brush thickness depends on the turbulence intensity tested. Specifically, the results show that, for relatively moderate value of turbulence intensity (see the second row in Fig. 9), increasing the fuel-air equivalence ratio increases the flame brush thickness. This is more pronounced at smaller mean bulk flow velocities and larger vertical distances from the flame-holder. This characteristic of moderately turbulent premixed V-shaped flames has been previously reported in the experimental investigations of Kheirkhah and Gülder [9], Namazian et al. [16], and Guo et al. [8]. The underlying physical mechanism associated with the increase of δ_T with ϕ is due to enhancement of reactants velocity fluctuations at the vicinity of the flame front. For further details associated with this phenomenon refer to [10].

In comparison to the results presented in Fig. 9d–f, those in Figure 9a–c show that, for small values of turbulence intensity, the flame brush thickness is almost insensitive to the fuel-air equivalence ratio. For relatively large values of turbulence intensity, the results in Fig. 9g–i does not show a trend for the effect of ϕ on δ_T. This characteristic of turbulent premixed flames is in agreement with prediction of the Langevin model/Taylor's turbulent diffusion theory [11–13] as well as the prediction of the level set formulation proposed in Peters [1]. It is argued in [1, 11–13] that the normalized flame brush thickness (δ_T/Λ) is dependent on the normalized convection time (t/τ). The following discussion examines the variation of δ_T/Λ with respect to t/τ.

Variation of the normalized flame brush thickness (δ_T) with the normalized convection time (t/τ) is presented in Fig. 10a. The results are shown for all experimental conditions tested along with results of [8, 9, 16]. For clarity purposes, only selected results from Kheirkhah and Gülder [9] are presented. The results from [9] are shown for limited

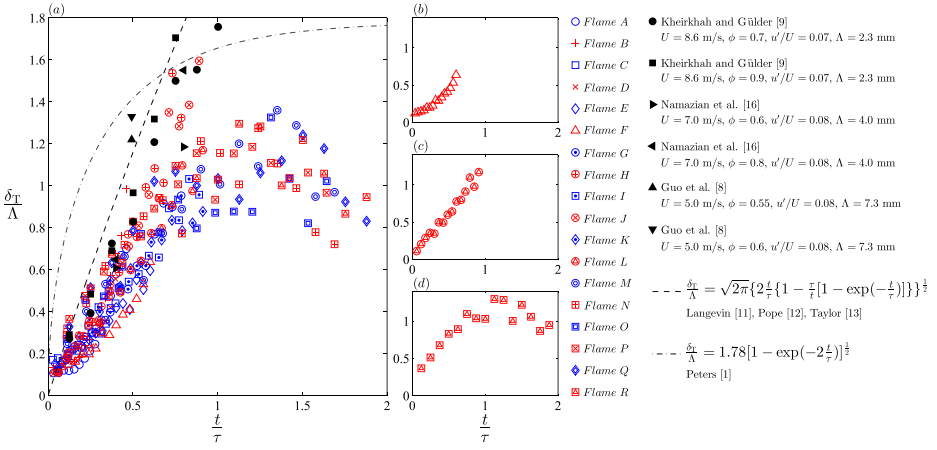

Fig. 10 **(a)** Variation of the normalized flame brush thickness with the normalized convection time. **(b)**, **(c)**, and **(d)** present the variations for Flames F, L and R conditions, respectively. The dashed line is the prediction of the Langevin model/Taylor's turbulent diffusion theory [11–13] and is given by: $\frac{\delta_T}{\Lambda} = \sqrt{2\pi}\{2\frac{t}{\tau}\{1 - \frac{\tau}{t}[1 - \exp(-\frac{t}{\tau})]\}\}^{\frac{1}{2}}$. The dotted-dashed line presents the formulation proposed in Peters [1] and is given by: $\frac{\delta_T}{\Lambda} = 1.78[1 - \exp(-2\frac{t}{\tau})]^{\frac{1}{2}}$

ranges of variation in the normalized flame brush thickness and the normalized convection time. Results for full range of variation are presented and discussed later. Also presented in Fig. 10a are the predictions of the Langevin model/Taylor's turbulent diffusion theory [11–13] as well as the formulation presented in Peters[1]. As can be seen from the results in the figure, δ_T/Λ features an increasing trend with t/τ. Due to scatter in the results presented, the effects of the governing parameters are not apparent. For this reason, representative variations are also presented in Fig. 10b–d. The results in the figures are shown for fixed values of fuel-air equivalence ratio ($\phi = 0.7$) and mean bulk flow velocity ($U = 8.3$ m/s). Data in Fig. 10b, c and d correspond to $u'/U = 0.02$, 0.06, and 0.17, respectively. As can be seen from the results in the figures, the rate of change of δ_T/Λ with t/τ depends on the turbulence intensity tested. For relatively small value of u'/U, see Fig. 10b, the variation is such that increasing t/τ increases the rate of change of δ_T/Λ. For moderately turbulent condition, that are the experimental conditions of Flames G-L, δ_T/Λ features a linear relation with t/τ. For relatively large value of u'/U, increasing the normalized convection time decreases the rate of change of the normalized flame brush thickness. This decrease is such that the normalized flame brush thickness data features a plateau for large values of u'/U. The plateau of the experimental results at large values of u'/U (see Flames M-R conditions) is similar to the trend predicted by the formulation proposed by Peters [1], see the dotted-dashed line in Fig. 10a.

The above arguments as well as previous experimental investigations [8, 9, 16] show that the mean bulk flow velocity (U), the fuel-air equivalence ratio (ϕ), the turbulence intensity (u'/U), and the integral length scale (Λ) can potentially affect the flame brush thickness of premixed methane-air V-shaped flames. This means that, for fixed values of U, ϕ, and u'/U, the normalized flame brush thickness data (δ_T/Λ) should collapse. In order to investigate this, similar experimental conditions from the results of the present study along with those from Kheirkhah and Gülder [9] were selected and presented in Fig. 11a–c. Figure 11a, b and c correspond to mean bulk flow velocities of 4.0, 6.2, and 8.3-8.6 m/s, respectively. In Fig. 11a–c, the turbulence intensities associated with the results of Kheirkhah and Gülder [9] and those of the present study are close, $u'/U \approx 0.06 - 0.08$. For the results in Fig. 11a–c, the fuel-air equivalence ratio is fixed at $\phi = 0.7$. The integral length scale associate with the conditions of the present study varies from 3.8 mm to 4.2 mm and that associated with [9] changes from 1.9 mm to 2.3 mm. The reason for the difference between

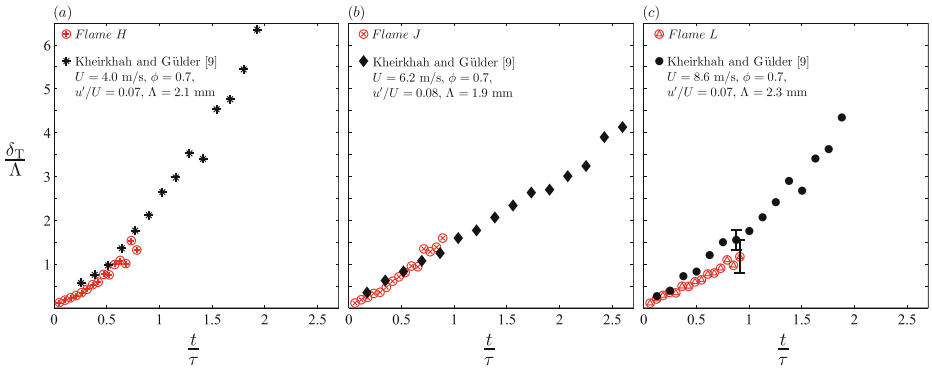

Fig. 11 Variation of the normalized flame brush thickness with the normalized convection time. The results are presented for the full range of variation in δ_T/Λ and t/τ. **(a)**, **(b)**, and **(c)** correspond to mean bulk flow velocities of $U = 4.0$, 6.2, and 8.3-8.6 m/s, respectively

the integral length scales of the present study and that pertaining to Kheirkhah and Gülder [9] is due to difference in position of the turbulence generator inside the nozzle section associated with the present study and that of [9]. The error bars in Fig. 11c pertain to the uncertainties associated with the corresponding experiments. As shown in Fig. 11a–c, the normalized flame brush thickness data almost collapse and follows a linear trend with t/τ. This is in agreement with the discussions presented earlier for moderately turbulent flames. The results also show that ranges of variation in δ_T/Λ and t/τ for the experiments are different. This is due to scaling caused by the variation in the integral length scales. In essence, the above arguments suggest that the normalized flame brush thickness is significantly dependent on the mean bulk flow velocity, the fuel-air equivalence ratio, and the turbulence intensity. For fixed values of U, ϕ, and u'/U, changing Λ has a scaling effect on the variation of δ_T/Λ with t/τ.

Kheirkhah and Gülder [9] investigated correlation between the flame brush thickness and the RMS of the flame front position. Their experiments [9] were performed for relatively moderate values of turbulence intensity. For this condition, their results [9] showed that the flame brush thickness is linearly correlated with the RMS of the flame front position. The correlation is independent of the values of mean bulk flow velocity, fuel-air equivalence ratio, and the integral length scale tested. Validity of the correlation between δ_T and x', for relatively large values of u'/U, has not been investigated in the past studies. In order to investigate this, variation of the flame brush thickness with RMS of the flame front position for all the experimental conditions tested are presented in Fig. 12. Representative results from Kheirkhah and Gülder [9] are shown in

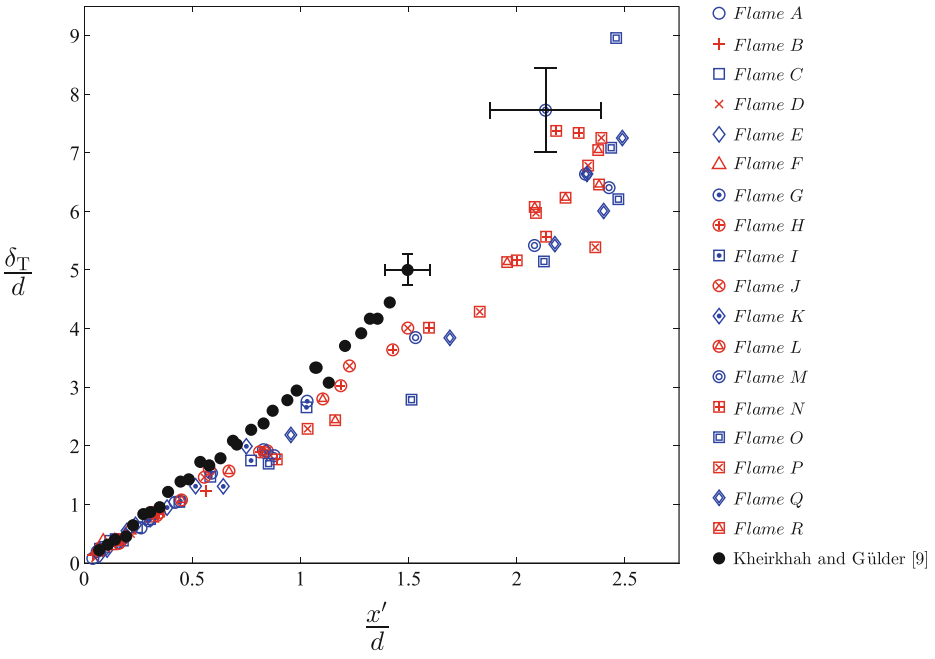

Fig. 12 Flame brush thickness and root-mean-square of the flame front position. The solid symbol correspond to the results from Kheirkhah and Gülder [9], with $\phi = 0.7$, $u'/U = 0.07$, and $\Lambda = 2.3$ mm

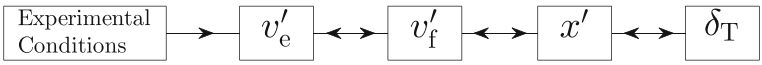

Fig. 13 Proposed block-based diagram for describing the mechanism associated with dynamics of turbulent premixed V-shaped flames

the figure as well. The results are normalized by the diameter of the flame-holder. The error bars in the figures pertain to uncertainties associated with the corresponding experiments. As can be seen from the results in the figure, the flame brush thickness follows a linear trend with RMS of the flame front position, independent of the experimental conditions tested.

For moderately turbulent premixed V-shaped flames, the characteristics of x' is argued to be linked to the characteristics of turbulent flow at the vicinity of the flame front and inside the reactants region [10]. Specifically, results of Kheirkhah and Gülder [10] show that changing the experimental conditions, e.g., ϕ, varies RMS of the transverse component of the reactants velocity at the vicinity of the flame front, referred to as RMS of the edge velocity (v'_e). This causes the RMS of the transverse component of the flame front velocity (v'_f) to change. The change in the RMS of the transverse component of the flame front velocity results in variation of the RMS of the flame front position. Also, it was shown that x' is linearly correlated with the flame brush thickness. The above argument is presented in a block-based diagram shown in Fig. 13. In the diagram the connections between v'_e, v'_f, x', and δ_T are presented using double-sided arrows, since these parameters can potentially feature mutual interactions. The connection between the experimental conditions and v'_e is presented as one-sided arrow since the statistics of edge velocity cannot change the experimental conditions tested. Note that validity of the connections between the parameters presented in Fig. 13 are experimentally investigated for moderate values of turbulence intensity. The experimental results in Fig. 12 showed that the correlation between δ_T and x' is similar for the range of turbulence intensities investigated. Thus, it is speculated that the mechanism proposed in [10], and elaborated in Fig. 13, can also potentially hold for the range of turbulence intensities investigated.

4 Concluding Remarks

Topology as well as brush thickness of turbulent premixed V-shaped flames were investigated experimentally using Mie scattering and Particle Image Velocimetry techniques. The experiments were performed for mean bulk flow velocities of 4.0, 6.2, and 8.3 m/s along with two fuel-air equivalence ratios of 0.6 and 0.7. A novel experimental apparatus, which allows for producing large values of turbulence intensities, was developed. Three turbulence intensities of approximately 2 %, 6 %, and 17 % were tested in the experiments.

For the relatively small value of turbulence intensity tested, the results show that the flame fronts either represent two straight lines or two perturbed lines with small size of perturbations. In both cases, the flame fronts are symmetric with respect to the vertical axis. In comparison to the results associated with small values of turbulence intensity, those pertaining to moderate value of this parameter show that the sizes of the wrinkles are significantly large and are not symmetric with respect to the vertical axis. The results show cusps formation for both relatively small and moderate turbulence intensities. It was argued that the vortices formed in the wake of the flame-holder can play a role in the cusp formation process. Increasing the turbulence intensity from about 6 % to approximately 17 % significantly

affects topology of the premixed flames. Specifically, the flame fronts feature: mushroom-shaped structures, freely propagating sub-flames, pocket formation, localized extinction, and horn-shaped structures.

Analysis of the results associated with the flame brush thickness shows that, for the experimental conditions tested, the turbulence intensity and the equivalence ratio can affect the flame brush thickness. The effect of equivalence ratio is limited to moderate values of turbulence intensity. Specifically, increasing the fuel-air equivalence ratio increases the flame brush thickness. The results show that increasing the turbulence intensity also increases the flame brush thickness. Specifically, at 20 mm above the flame-holder, increasing the turbulence intensity from about 2 % to 17 % increases the flame brush thickness by one order of magnitude.

In order to compare the result of the present study with those of the literature, variation of the normalized flame brush thickness (δ_T/Λ) with the normalized convection time (t/τ) was investigated. The results show that the values of the normalized flame brush thickness do not collapse. Also, the trend of variation of δ_T/Λ with t/τ is significantly dependent on the turbulence intensities examined. However, analysis of the flame brush thickness data along with the RMS of the flame front position show that these parameters are correlated and follow a linear trend for all experimental conditions tested. Although this characteristic was previously reported for moderately turbulent V-shaped flames, the present study extends it to a relatively wide range of turbulence intensities. Comparison of the results of the present study and those of Kheirkhah and Gülder [9, 10] suggests that the underlying physics associated with the interaction of turbulent flow and premixed flames can potentially hold for a wide range of turbulence intensities.

Acknowledgments The authors are grateful for financial support from the Natural Sciences and Engineering Research Council (NSERC) of Canada.

References

1. Peters, N.: Turbulent Combustion, 1st Edition. Cambridge University Press (2000)
2. Glassman, I., Yetter, R.A.: Combustion, 4th Edition. Elsevier Inc. (2008)
3. Clavin, P.: Dynamic behavior of premixed flame fronts in laminar and turbulent flows. Prog. Energy Combust. Sci. **11**, 1–59 (1985)
4. Driscoll, J.F.: Turbulent premixed combustion: Flamelet structure and its effect on turbulent burning velocities. Prog. Energy Combust. Sci. **34**, 91–134 (2008)
5. Koutmos, P., McGuirk, J.J.: Isothermal flow in a gas turbine combustor–a benchmark experimental study. Exp. Fluids **7**, 344–354 (1989)
6. Goix, P., Paranthoen, P., Trinite, M.: A tomographic study of measurements in a V-shaped H_2-air flame and a Lagrangian interpretation of the turbulent flame brush evolution. Combust. Flame **81**, 229–241 (1990)
7. Gouldin, F.C., Hilton, S.M., Lamb, T.: Experimental evaluation of the fractal geometry of flamelets. Proc. Combust. Inst. **22**, 541–550 (1988)
8. Guo, H., Tayebi, B., Galizzi, C., Escudié, D.: Burning rates and surface characteristics of hydrogen-enriched turbulent lean premixed methane-air flames. Int. J. of Hydrog. Energy **35**, 11342–11348 (2010)
9. Kheirkhah, S., Gülder, Ö.L.: Turbulent premixed combustion in V-shaped flames: Characteristics of flame front. Phys. Fluids **25**, 055107 (2013)
10. Kheirkhah, S., Gülder Ö. L.: Influence of edge velocity on flame front position and displacement speed in turbulent premixed combustion. Combust. Flame. doi:10.1016/j.combustflame.2014.04.008
11. Langevin, P.: Sur la théorie du mouvement brownien. C. R. Acad. Sci. Paris **146**, 530–533 (1908)
12. Pope, S.B.: Turbulent Flows. Cambridge University Press (2000)
13. Taylor, G.I.: Diffusion by continuous movements. Proc. Lond. Math. Soc. **20**, 196–212 (1922)

14. Lipatnikov, A.N., Chomiak, J.: Turbulent flame speed and thickness: phenomenology, evaluation, and application in multi-dimensional simulations. Prog. in Energy Combust. Sci. **28**, 1–74 (2002)
15. Renou, B., Mura, A., Samson, E., Boukhalfa, A.: Characterization of the local flame structure and the flame surface density for freely propagating premixed flames at various Lewis numbers. Combust. Sci. Technol. **174**, 143–179 (2002)
16. Namazian, M., Shepherd, I.G., Talbot, L.: Characterization of the density fluctuations in turbulent V-shaped premixed flames. Combust. Flame **64**, 299–308 (1986)
17. Rajan, S., Smith, J.R., Rambach, G.D.: Internal structure of a turbulent premixed flame using Rayleigh scattering. Combust. Flame **57**, 95–107 (1984)
18. Eckbreth, A.C.: Laser diagnostics for combustion temperature and species, 2nd Edition. Overseas Publishers Association (1996)
19. Gülder, Ö.L.: Contribution of small scale turbulence to burning velocity of flamelets in the thin reaction zone regime. Proc. Combust. Inst. **31**, 1369–1375 (2007)
20. Smallwood, G.J., Gülder, Ö.L., Snelling, D.R., Deschamps, B.M., Gökalp, I.: Characterization of flame front surfaces in turbulent premixed methane/air combustion. Combust. Flame **101**, 461–470 (1995)
21. Peters, N.: Laminar flamelet concepts in turbulent combustion. Proc. Combust. Inst. **21**, 1231–1250 (1986)
22. Yu, G., Law, C.K., Wu, C.K.: Laminar flame speeds of hydrocarbon + air mixtures with hydrogen addition. Combust. Flame **63**, 339–347 (1986)
23. Bradley, D., Lau, A.K.C., Lawes, M.: Flame stretch rate as a determinant of turbulent burning velocity. Philos. Trans. R. Soc. Lond. **338**, 359–387 (1992)
24. Shanbhogue, S.J., Shin, D.-H., Hemchandra, S., Plaks, D., Lieuwen, T.: Flame sheet dynamics of bluff-body stabilized flames during longitudinal acoustic forcing. Proc. Combust. Inst. **32**, 1787–1794 (2009)
25. Lee, T.W., North, G.L., Santavicca, D.L.: Surface properties of turbulent premixed propane/air flames at various Lewis numbers. Combust. Flame **93**, 445–456 (1993)
26. Hertzberg, J.R., Shepherd, I.G., Talbot, L.: Vortex shedding behind rod stabilized flames. Combust. Flame **86**, 1–11 (1991)
27. Buchmann, A., Dinkelacker, F., Schäfer, T., Schäfer, M., Wolfrum, M.: Measurement of the instantaneous detailed flame structure in turbulent premixed combustion. Proc. Combust. Inst. **26**, 437–445 (1996)
28. Coriton, B., Frank, J.H., Hsu, A.G., Smooke, M.D., Gomez, A.: Effect of quenching of the oxidation layer in highly turbulent counterflow premixed flames. Proc. Combust. Inst. **33**, 1647–1654 (2011)
29. Cheng, R.K., Shepherd, I.G., Bédat, B., Talbot, L.: Premixed turbulent flame structures in moderate and intense isotropic turbulence. Combust. Sci. Technol. **174**, 29–59 (2002)
30. Shanbhogue, S.J., Husain, S., Lieuwen, T.: Lean blowoff of bluff body stabilized flames: Scaling and dynamics. Prog. Energy Combust. Sci. **35**, 98–120 (2009)
31. Yamaguchi, S., Ohiwa, N., Hasegawa, T.: Structure and blow-off mechanism of rod-stabilized premixed flame. Combust. Flame **62**, 31–41 (1985)
32. Kim, W.-W., Lienau, J.J., Van Slooten, P.R., Colket, M.B., III, Syed, M.R.E.S.: Towards modeling lean blow out in gas turbine flameholder applications. J. Eng. Gas Turbines Power **128**, 40–48 (2006)
33. Steinberg, A.M., Driscoll, J.F.: Straining and wrinkling processes during turbulence-premixed flame interaction measured using temporally-resolved diagnostics. Combust. Flame **156**, 2285–2306 (2009)